JOURNAL OF MATERIALS SCIENCE **38** (2003) 2793–2801

Mapping of thermoplastic elastomeric nitrile rubber/poly(styrene-co-acrylonitrile) blends using tapping mode atomic force microscopy and transmission electron microscopy

S. ANANDHAN, P. P. DE, S. K. DE
Rubber Technology Center, Indian Institute of Technology, Kharagpur 721 302, West Bengal, India

S. BANDYOPADHYAY
School of Materials Science and Engineering, University of New South Wales, Sydney 2052, Australia

A. K. BHOWMICK*
Rubber Technology Center, Indian Institute of Technology, Kharagpur 721 302, West Bengal, India
E-mail: anilkb@rtc.iitkgp.ernet.in

Dynamically vulcanized thermoplastic elastomeric blends of nitrile rubber (NBR)/poly(styrene-co-acrylonitrile) (SAN) were mapped by tapping mode atomic force microscopy (TMAFM) and transmission electron microscopy (TEM). The morphology changes with the blend ratio and dynamic vulcanization. Roughness and surface analysis were used to study the effect of dynamic vulcanization and mixing sequence on the surface texture of the thermoplastic elastomeric blends. Surface geometry was quantified by power spectral density (PSD) and fractal analysis.

1. Introduction

Immiscible polymer blends have heterophase morphology. The morphology of various polymer blends was discussed in the literature [1]. Thermoplastic elastomers derived from rubber-plastic blends have rubber as the dispersed phase in a matrix of plastic [2, 3]. The size of the dispersed rubber phase is in the micrometer range. Microscopy and spectroscopic techniques including X-ray photoelectron spectroscopy, secondary ion mass spectrometry, near field scanning optical microscopy, electron microscopy, neutron and X-ray scattering and reflection optical microscopy have been used either in combination or independently to provide information about morphology and comparison of multicomponent polymer systems [4–7]. However, these techniques lack the lateral resolution needed to detect heterogeneity in polymer blends. In addition, these techniques require a specific sample preparation procedure so that the sample is amenable for assay with the technique.

One technique that can provide direct spatial mapping of surface topography and surface heterogeneity with nanometer resolution is atomic force microscopy (AFM) [7, 8]. In AFM, a probe consisting of a sharp tip (nominal tip radius on the order of 10 nm) located near the end of a cantilever beam is scanned across the sample surface using piezoelectric scanners. Changes in the tip-sample interaction are often monitored using an optical lever detection system, in which a laser is reflected off the cantilever and onto a position sensitive photodiode. During scanning, a particular operating parameter is maintained at a constant level, and images are generated through a feed back loop between the optical detection system and the piezoelectric scanners.

Three imaging modes can be used to produce topographic images of sample surfaces, namely, contact mode, non-contact mode, and tapping mode AFM (TMAFM). TMAFM tends to be more applicable to general imaging of soft samples, such as biological and polymeric materials, under ambient conditions [9, 10] and is used exclusively in the work described in this paper.

Ganter *et al.* [11] utilized AFM in the studies on poly(propylene)/poly(olefin) blends and polybutadiene (BR)/styrene-butadiene rubber (SBR) blends. Mass *et al.* [12] examined crosslinked BR/butyl rubber (IIR), SBR/IIR, and SBR/BR blends using AFM. Microphase domains of styrene-ethylene-butylene-styrene (SEBS) triblock copolymers were studied by using AFM by Motomatsu *et al.* [13]. Biodegradable polymer blends of poly(sebacic anhydride)/poly(DL-lactic acid)

*Author to whom all correspondence should be addressed.

were characterized with the aid of AFM by Davies *et al.* [14]. Buchko *et al.* [15] studied quantitatively the surfaces of porous, biocompatible protein polymer thin films by TMAFM. They used power spectral density (PSD) analysis to evaluate fractal values of the surfaces of those films. From our laboratory, AFM data on several systems [16–18] have been reported.

Anandhan *et al.* [19] reported the effect of mixing sequence and dynamic vulcanization on mechanical and dynamic mechanical properties of thermoplastic elastomeric nitrile rubber (NBR)/poly(styrene-co-acrylonitrile) (SAN) blends (70:30 w/w ratio). The mechanical properties of the blends prepared by blending of NBR-curatives master batch to softened SAN were superior to those prepared by adding curatives to a softened preblend of NBR and SAN. The blends of NBR/SAN were found to be immiscible and heterophasic in nature. In this paper, the morphology of dynamically vulcanized NBR/SAN blends is discussed by using TMAFM and transmission electron microscopy (TEM). An attempt has been made to correlate fractal values (obtained from PSD) with the mechanical properties of the blends prepared by different mixing sequences. The effect of blend ratio on morphology is also reported.

2. Experimental

2.1. Materials

The details of the materials used are shown in Table I.

2.2. Preparation of the blends

The 60/40 and 70/30 (w/w ratio) blends of NBR/SAN were prepared (denoted as B_6 and B_7). The dynamically vulcanized counterparts of B_6 and B_7 (designated as $B_6S_{0.75}$, and $B_7S_{0.75}$ respectively, $S_{0.75}$ denoting presence of 0.75 phr of sulfur) were also prepared. All the formulations are discussed below. In our earlier communication [19], the effect of mixing sequence and dynamic vulcanization on mechanical properties of NBR/SAN blends was reported.

TABLE I Details of the materials used

Material	Supplier/manufacturer
NBR Grade: N553NS ACN content: 34% Mooney viscosity: ML_{1+4} at 100°C, 46 M_v: 2.39×10^5 (viscometry)	Apar Industries Ltd., India.
SAN Grade: Lustron sparkle ACN content: 27% M_w: 1.65×10^5 (GPC) MFI: 1.91 g/10 min at 200°C under a load of 2.16 kg	Monsanto, USA
Zinc oxide[a]	E-Merck, Mumbai, India
Stearic acid[a]	Local supplier
MBT[a,b]	ICI Ltd., Rishra, India
TMTD[a,c]	ICI Ltd., Rishra, India
Sulfur	Qualigens, Mumbai, India

[a]Rubber grade.
[b]Mercapto benzothiazole (accelerator).
[c]Tetramethyl thiuram disulfide (accelerator).

The blends were prepared by mixing of NBR and SAN in a Brabender Plasticorder PLE 330 at 180°C and 60 rpm with cam type rotors. After mixing, the blends were removed in hot condition and sheeted out in a water-cooled two roll mill (Schwabenthan, Germany) at 25°C. Sheeted out blends were compression molded between polyester sheets at 210°C in a hydraulic press (Moore press, Birmingham, England) at a pressure of 5 MPa for 2 min. Then, the platens were cooled under pressure.

The mixing was done according to three different schemes. 70/30 (w/w) blend of NBR/SAN [curing system: zinc oxide, 3; stearic acid, 2; mercapto benzothiazole (MBT), 1; tetramethyl thiuram disulfide (TMTD), 0.5; sulfur, 0.75; the figures are in phr based on the NBR phase] was used in this study.

Scheme 1: NBR was charged in the Brabender Plasticorder at 70°C. Sulfur, zinc oxide and stearic acid were added. Mixing was done at 60 rpm for 4 min. The rubber compound was passed through a two-roll mill. MBT and TMTD were added and the rubber masterbatch was prepared. SAN was softened in the Brabender Plasticorder at 180°C for 2 min. The rubber masterbatch was added to the softened SAN and mixed at 60 rpm for 4 min (by which time, the torque stabilized). The mixture was sheeted out in a cold two-roll mill and cut in to strips. The strips were remixed for 2 min in the Brabender Plasticorder and sheeted out in the mill. This blend is designated as $B_7S_{0.75}$. Blend $B_6S_{0.75}$ was also prepared in the same manner. The formulation of $B_6S_{0.75}$ is as follows: NBR, 60; SAN, 40; MBT, 1; TMTD, 0.5; sulfur, 0.75; the dosages of curatives are in phr based on the NBR phase.

Scheme 2: SAN was softened in the Brabender Plasticorder at 180°C for 2 min. Strips of NBR were added and mixed at 60 rpm for 1 min. Zinc oxide, stearic acid, and MBT/TMTD were added followed by sulfur. Mixing was continued for 3 min. The mixture was sheeted out and remixed as described earlier. This blend is designated as $B_7S_{0.75}PB$.

Scheme 3: Mixing was done as described in Scheme 2 but time of mixing was extended by 2 min, i.e., for a total time of 8 min. The mixture was sheeted out and remixed as described earlier. This blend is designated as $B_7S_{0.75}PB_8$.

The mechanical properties of these blends are given in Table II.

2.3. Morphology of the blends

2.3.1. Transmission electron microscopy (TEM) studies

TEM studies of the blends were carried out by using a Hitachi H-7000 transmission electron microscope at an accelerating voltage of 75 kV and a beam current of 10 μA.

The samples of about 50 nm thickness were prepared by cryomicrotoming of the samples ($B_7S_{0.75}$,

TABLE II Mechanical properties of the NBR/SAN blends

Sample designation	Tensile strength (MPa)	Elongation @ break (%)	Modulus @ 100% elongation (MPa)	Modulus @ 200% elongation (MPa)	Tension set @ 100% elongation (%)
$B_7S_{0.75}$	11.9	267	6.7	9.6	24
$B_7S_{0.75}PB$	8.8	250	5.4	7.8	20
$B_7S_{0.75}PB_8$	6.5	190	5.7	—	32
$B_6\ S_{0.75}$	14.5	264	10.2	13.2	45
B_6	6.2	150	5.3	—	50
B_7	2.2	191	2.1	—	38

$B_7S_{0.75}PB$, $B_7S_{0.75}PB_8$) in a Reichert-Jung Ultramicrotome using glass knives (made using LKB Bromma 7800 knife maker), after freezing the specimens below their glass transition temperature (−40°C) using liquid nitrogen. The cryomicrotomed specimens were transferred to copper grids (200 mesh size) by using a tweaser. The grids were kept on glass slides and preserved in a petridish covered with a lid.

The rubber phase (NBR) in the specimens was stained by a 2% solution of osmium tetroxide (osmium tetroxide in sodium cacodylate) for a period of 24 h.

2.3.2. Atomic force microscopy (AFM) studies

Cryomicrotoming was done in the Reichert-Jung Ultramicrotome, by using the same procedure as described under TEM. Average sample thickness was, however, 30 μm.

AFM studies were carried out in air at ambient conditions (25°C) using Dimension 3000 Atomic Force Microscope (Digital Instruments, Santa Barbara, CA, USA). Topographic (height), phase (phase contrast), and amplitude images were recorded in the tapping mode (TMAFM). The TMAFM experiment and phase and amplitude imaging have been described in detail elsewhere [20, 21]. This mode is well suited to the study of soft polymers such as elastomers. In tapping mode, the cantilever oscillates very near its resonance frequency, so that the tip makes contact with the sample surface only briefly in each cycle of oscillation. This short intermittent tip-sample contact reduces lateral forces during scanning, thus preventing sample damage.

Usually, the feed back mechanism in TMAFM is controlled by the set point ratio defined as $r_s = A_s/A_o$, where A_s is the set point amplitude maintained by adjusting the vertical position of the sample, and A_o is the amplitude of the cantilever's free oscillation. In this study, a set point ratio of 0.8–0.9 (light tapping) was employed.

Scanning was done using etched silicon tips (OTESPA probe), each with a nominal tip radius of curvature of 5–10 nm and spring constant in the range of 20–100 N/m. The cantilever was oscillated at its resonance frequency, which ranged between 200 and 400 kHz. All the images were recorded using free oscillation amplitude of 140 ± 10 nm. The general characteristics of the probes are: cantilever length, 125 μm; cantilever configuration, single beam; reflective coating, none; sidewall angles, 17° side, 25° front and 10° back. All the images contained 512 data points. Scan area was $10 \times 10\ \mu m^2$. For each sample, a minimum of 3 images were analyzed. The analysis was performed using Nanoscope III-a software version 4. The bows in the raw images were removed using the operation called flattening, which would eliminate the unwanted features from the images by calculating a second order least squares fit of the selected segment, then subtracting it from the scan line.

2.3.2.1. Roughness analysis. While doing the roughness analysis, the flattened images were subjected to a second order plane fit in order to remove the tilt and distortions in the images. Roughness consists of fine irregularities of the surface texture. The most commonly used roughness indicators are root mean square roughness R_{ms} and R_a. The R_{ms} roughness is defined as the square root of the mean value of the square of the distances Z_i of the points i from the mean surface level:

$$R_{ms} = \left(1/N \times \sum Z_i^2\right)^{1/2} \quad (1)$$

The mean surface level is defined as the line about which roughness is measured. It is parallel to the general direction of the profile within the limits of the sampling length, such that the sums of the areas contained between this line and those parts of the profile that lie on either side are equal. Assuming surface height variation is measured as Z_i in the $\pm Z$ direction, mathematically the mean surface level is defined to satisfy the following equation:

$$\sum Z_i = 0 \quad (2)$$

The average roughness R_a is the average of the absolute values of the surface height variations Z_i measured from the mean surface level, as given by the following equation:

$$R_a = 1/N \times \sum |Z_i| \quad (3)$$

Generally, if a surface is flat and contains no large deviations from the mean surface level, R_{ms} and R_a will be similar. However, if a surface is very rough and there are appreciable numbers of large bumps and holes, the value of Z_i will dominate the surface statistics and R_{ms} will be larger than R_a [22].

2.3.2.2. Section analysis. Depth, height, width, and angular measurements can be easily made with section analysis. A cross sectional line was drawn across any part of the image, and the vertical profile along that line was displayed. Up to three pairs of cursors were placed on the line section at any point to make horizontal, vertical, and angular measurements. The cursor was used to determine the predominant periodicities along the cross section by placing it at peaks in the spectrum.

2.3.2.3. Power spectral density. The power spectral density function (PSD) is useful in analyzing surfaces. The function reveals periodic surface features,

which might otherwise appear random, and provides a graphic representation of how such features are distributed. Power is roughness amplitude squared. The power spectrum is a plot of power as a function of spatial wavelength or frequency. The power spectral density is a plot of density, in spatial frequency space of the power spectrum [23].

In order to understand surface analysis in the context of the PSD, it is necessary to consider surfaces as the superposition of spatial waves. The combination of waves of different spatial frequencies (or wavelengths) can be thought of as a hypothetical surface profile. The wavelength is given in μm, and the spatial frequency (f) is the inverse of the wavelength so that large wavelengths correspond to low frequency. The variations of height fluctuations in real space can be analyzed in terms of the power spectrum in frequency space through the use of Fourier transform, which is a well known means of relating real space to frequency space. In the one-dimensional (1D) case of $h(x)$, where $H(f)$ is the resulting frequency space profile of the real surface, the Fourier transform can be written as

$$H(f) = 1/L \int h(x) \exp(-2\pi i f x)\, \mathrm{d}x \qquad (4)$$

where, L is the total length of the scan and 'i' is $\sqrt{-1}$. This quantity $[H(f)]$ is then squared to determine the power of the surface, P. The PSD is then defined as

$$\mathrm{PSD} = P/\Delta f \qquad (5)$$

Δf is the change in frequency. The units of (length)^3 are used for the 1D PSD.

The physical consequence of applying this analysis is presented in Fig. 1 using both a periodic and randomly rough surface. The surfaces were analyzed by a series of line scans of N_x steps yielding a profile, $h(x)$, for each value from 1 to N_y in the y direction. The PSD was then calculated by taking the Fourier transform of each of these line scans, squaring the result to determine the power, and averaging the power calculated for each line scan to generate a single 1D PSD for the surface. Plotting log (Power) versus log (frequency) reveals characteristic dimensions for the periodic surface in the form of peaks. The frequency value at the center of the peak is related to the real space value of the wavelengths that define this periodic surface. The second case is that of a self-affine surface. This randomly rough surface had a transition point between frequency-independent behavior at low frequency and a self-similar roughness at higher frequency. The physical meaning of the flat part of the curve at low frequency was that across these dimensions in real space, there was no significant deviation in the value of $h(x, y)$. However, below the transition point, $h(x, y)$ varied in a constant manner.

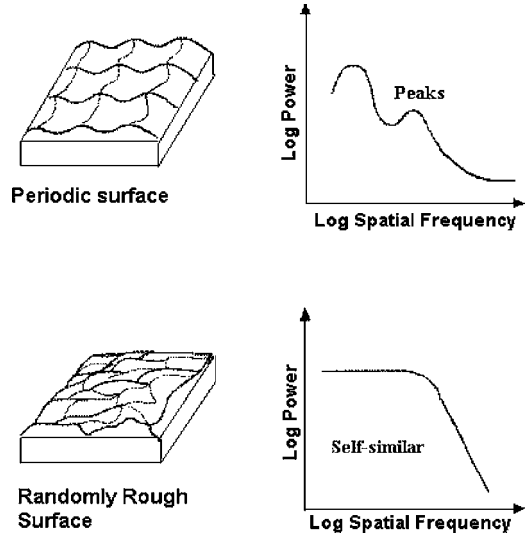

Figure 1 Schematic of the use of power spectral density. Plotting the power of a surface versus the frequency reveals spatial frequency behavior characteristic of the surface type. Periodic surfaces have peaks while randomly rough surfaces show a transition from a self-similar, constant slope region to a smooth region.

2.3.2.4. Mathematical descriptions of surfaces. The constant slope regimes of the PSD were described above as self-similar, which is a property of fractal objects. The fractal dimension method can give a detailed description of the domain distribution and orientation. It shows how a broken surface is, but it does not provide detailed height information.

According to the dimensions of Euclidean geometry, the integers 0, 1, 2, and 3 correspond to dots, lines, planes, and bodies respectively [22]. However, this simple classification is only suitable for regularly shaped objects. There are many examples of very irregular shape substances and artificial geometrical objects. In order to organize and compare such objects, one can intuitively assign intermediate dimensional values to them. For example, a broken line could have a dimension between 0 and 1, and jagged curve, which partly fills a certain plane, could have a dimension between 1 and 2. Kamal *et al.* [22] used the non-integer "fractal dimension" that was introduced by Mandelbrot, for the characterization of blown polyethylene (PE) films.

3. Results and discussion

3.1. Morphology of the NBR/SAN blends

3.1.1. TEM studies

Fig. 2a–c show the morphology of the dynamically vulcanized 70/30 NBR/SAN blends prepared by three different schemes ($B_7S_{0.75}$, $B_7S_{0.75}PB$, and $B_7S_{0.75}PB_8$). The black phase is the osmium tetroxide stained rubber phase. The dynamically vulcanized NBR/SAN blends contain NBR particles as the dispersed phase in a matrix of SAN. The dynamically vulcanized 60/40 NBR/SAN blend ($B_6S_{0.75}$) also possesses a similar morphology [Fig. 2d]. The size of the dispersed NBR particles in $B_7S_{0.75}$ is in the range of 0.5–1 μm. The dispersion is uniform. In the case of $B_7S_{0.75}PB$, and $B_7S_{0.75}PB_8$, the same is in the range of 0.4–0.6 μm, and for $B_6S_{0.75}$ the value in the range of 0.5–1 μm is registered. In our earlier studies using Scanning Electron Microscopy (SEM) [19], a similar morphology has been observed and the dimension of the dispersed phase is in line with the above range.

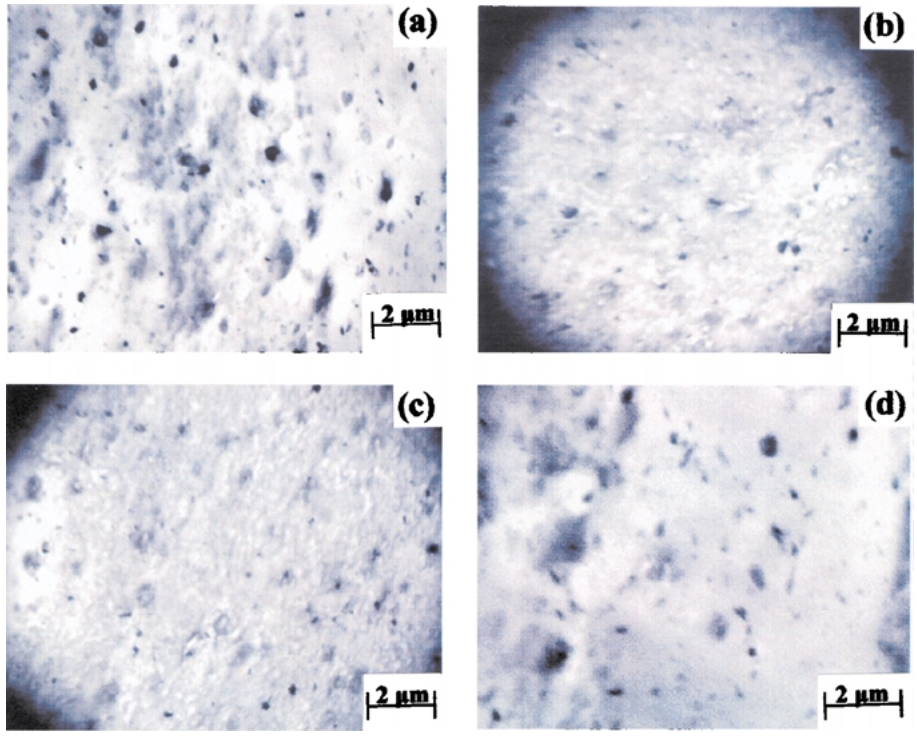

Figure 2 TEM photomicrographs of the blends: (a) $B_7S_{0.75}$, (b) $B_7S_{0.75}PB$, (c) $B_7S_{0.75}PB_8$, and (d) $B_6S_{0.75}$.

3.1.2. AFM studies

3.1.2.1. Interpretation of the AFM images. The AFM phase, amplitude and topographic (3-D height) images of the dynamically vulcanized blends $B_7S_{0.75}$, $B_7S_{0.75}PB$, $B_7S_{0.75}PB_8$, and $B_6S_{0.75}$ are shown in Fig. 3a–d. In the phase and amplitude images, a large number of "islands" are seen. These "islands" correspond to the dispersed NBR phase, following TEM observations. In general, assigning chemical composition to the features observed in height and phase images is

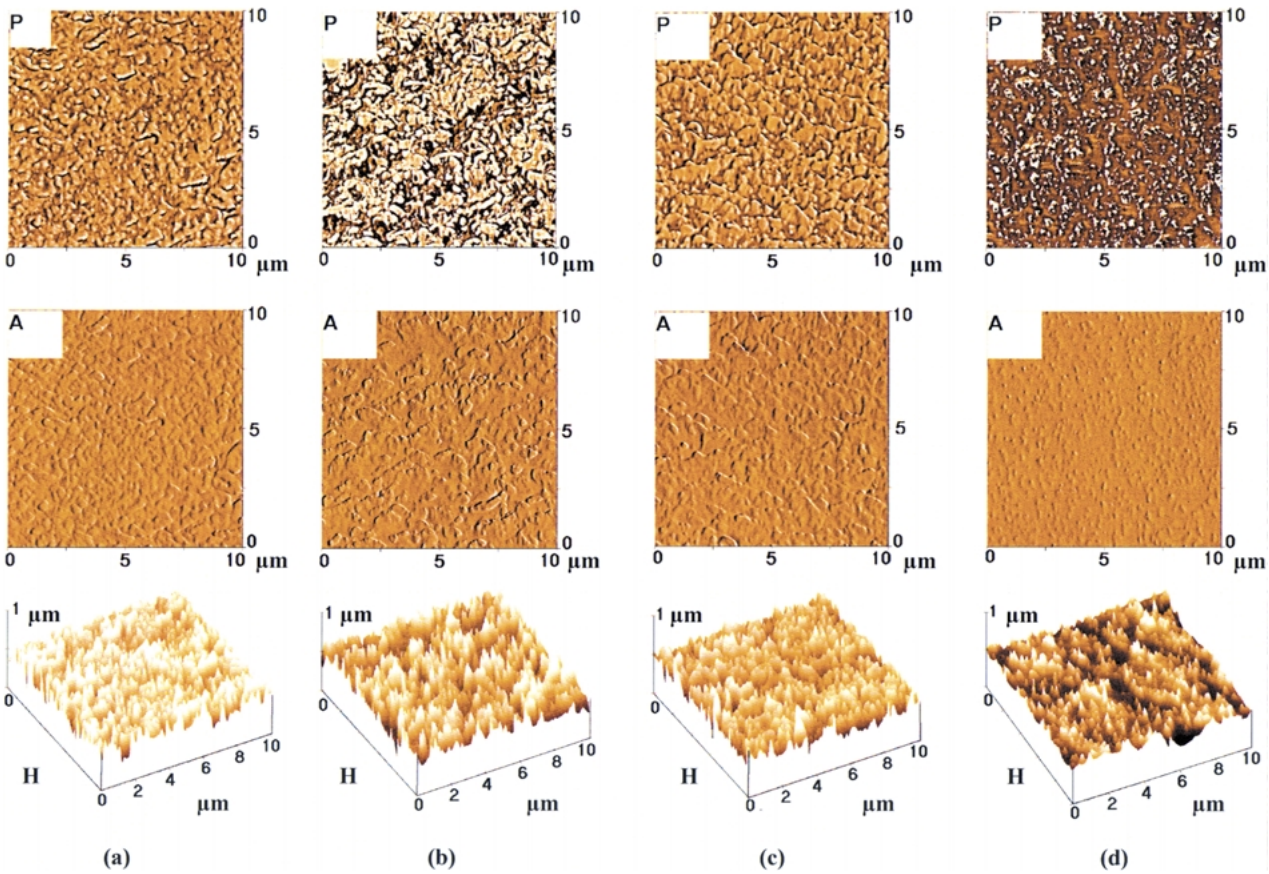

Figure 3 AFM phase (P), amplitude (A) and topographic (3-D height) (H) images of the blends: (a) $B_7S_{0.75}$, (b) $B_7S_{0.75}PB$, (c) $B_7S_{0.75}PB_8$, and (d) $B_6S_{0.75}$.

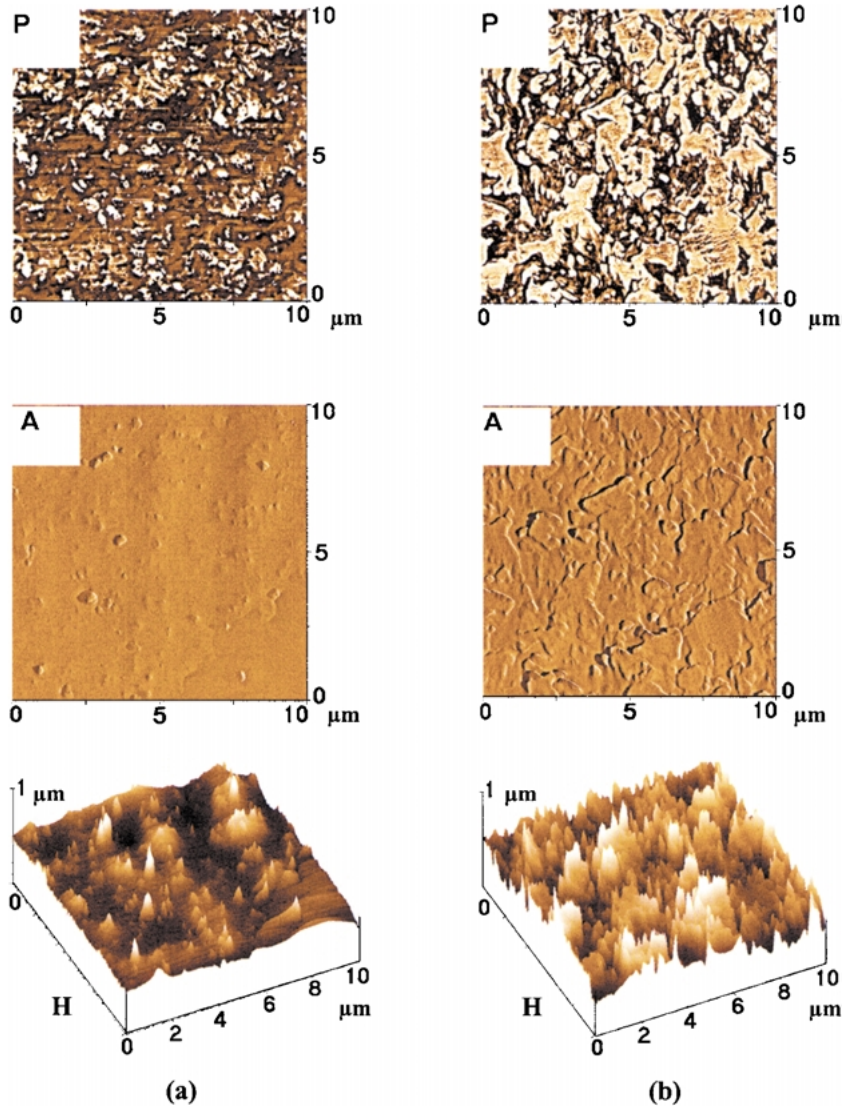

Figure 4 AFM phase (P), amplitude (A) and topographic (3-D height) (H) images of the blends: (a) B_6 and (b) B_7.

difficult unless additional experimentation is conducted [24]. Further, assignment of the bright or dark contrast to the hard or soft domain in phase imaging is not always straightforward. For example, several studies have assigned the brighter contrast to the stiffer material and the darker contrast to the softer material [25, 26]. In other reports, the darker region has been attributed to the harder material and the lighter region to the softer material [24, 27]. But, we have assigned the brighter regions to NBR based on TEM photomicrographs of the corresponding blends. In these blends, dynamically vulcanized NBR particles form the dispersed phase in a matrix of SAN.

The two-dimensional phase, amplitude and three-dimensional topographic (height) images of the corresponding unvulcanized blends, B_6 and B_7, are shown in Fig. 4a and b. The phase image of B_6 shows dispersed NBR particles in a matrix of SAN. The phase image of B_7 shows a co-continuous morphology. The dispersed NBR particles in B_6 are in the range of 0.5–1.2 μm, whereas in B_7 the same is in the range of 1–2 μm. The SEM and dynamic mechanical thermal analysis (DMTA) results also support these observations [19].

3.1.2.2. Section analysis. The vertical distance of the surface projections was measured by the use of cursors of different colors (denoted as A, B, C, D, E, and F). The line profiles of the blends $B_7S_{0.75}$, $B_7S_{0.75}PB$, $B_7S_{0.75}PB_8$, and $B_6S_{0.75}$ are presented in Fig. 5a–d. The vertical distances of the surface projections are presented in Table III. The blend $B_7S_{0.75}$ exhibits superior mechanical properties than $B_7S_{0.75}PB$ and $B_7S_{0.75}PB_8$ (Table II). This may be due to the smoothness of distribution of the dispersed phase. The TEM photomicrograph also shows uniformly dispersed NBR particles in

TABLE III Section analysis and fractal values of the blends

Blend designation	Vertical distance of the surface projections from the mean plane (nm)			Total fractal dimension (D_s) of the surface
	A-B	C-D	E-F	
$B_7S_{0.75}$	664	469	820	2.56
$B_7S_{0.75}PB$	488	547	1110	2.46
$B_7S_{0.75}PB_8$	371	820	977	2.45
$B_6S_{0.75}$	469	586	449	2.47
B_6	469	586	449	2.19
B_7	625	371	420	2.31

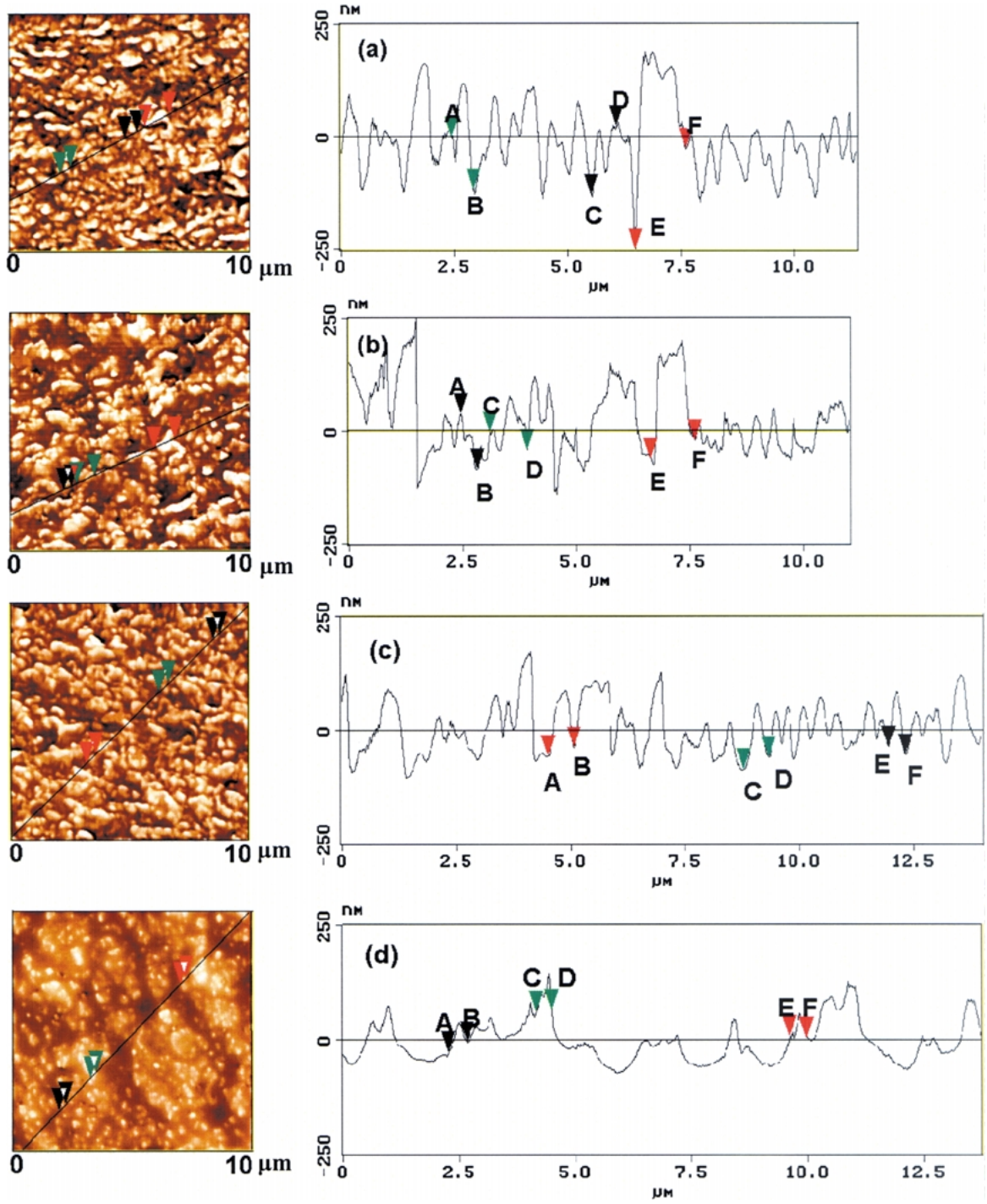

Figure 5 Line profiles of the blends: (a) $B_7S_{0.75}$, (b) $B_7S_{0.75}PB$, (c) $B_7S_{0.75}PB_8$, and (d) $B_6S_{0.75}$.

the SAN matrix. The blends B_6 and B_7 have a number of small projections on the surface (not shown here). All these are quantified and discussed in the next section.

3.1.2.3. Roughness and PSD. The R_{ms}, and R_a values of the dynamically vulcanized blends along with those of the unvulcanized blends are shown in Table IV. The R_{ms} and R_a values are not similar. It can be concluded that the surfaces of these blends are very rough and there are appreciable numbers of bumps and holes. The line profiles obtained from the section analysis also supports the above observation [Fig. 5a–d]. The R_{ms} and R_a values of the dynamically vulcanized blends are much higher than those of the unvulcanized blends.

Quantitative analysis of the surfaces of these blends is done by using the one dimensional PSD values. Log (power) versus Log (frequency) plots were prepared and the slopes (D) of the self-similar constant slope regions were determined by linear fitting using *Ori-*

TABLE IV Roughness values of the blends

Blend designation	R_{ms} (nm)	R_a (nm)
$B_7S_{0.75}$	73.5	60.1
$B_7S_{0.75}PB$	75.5	60.5
$B_7S_{0.75}PB_8$	54.0	44.9
$B_6S_{0.75}$	70.0	55.7
B_6	37.3	29.6
B_7	48.4	37.5

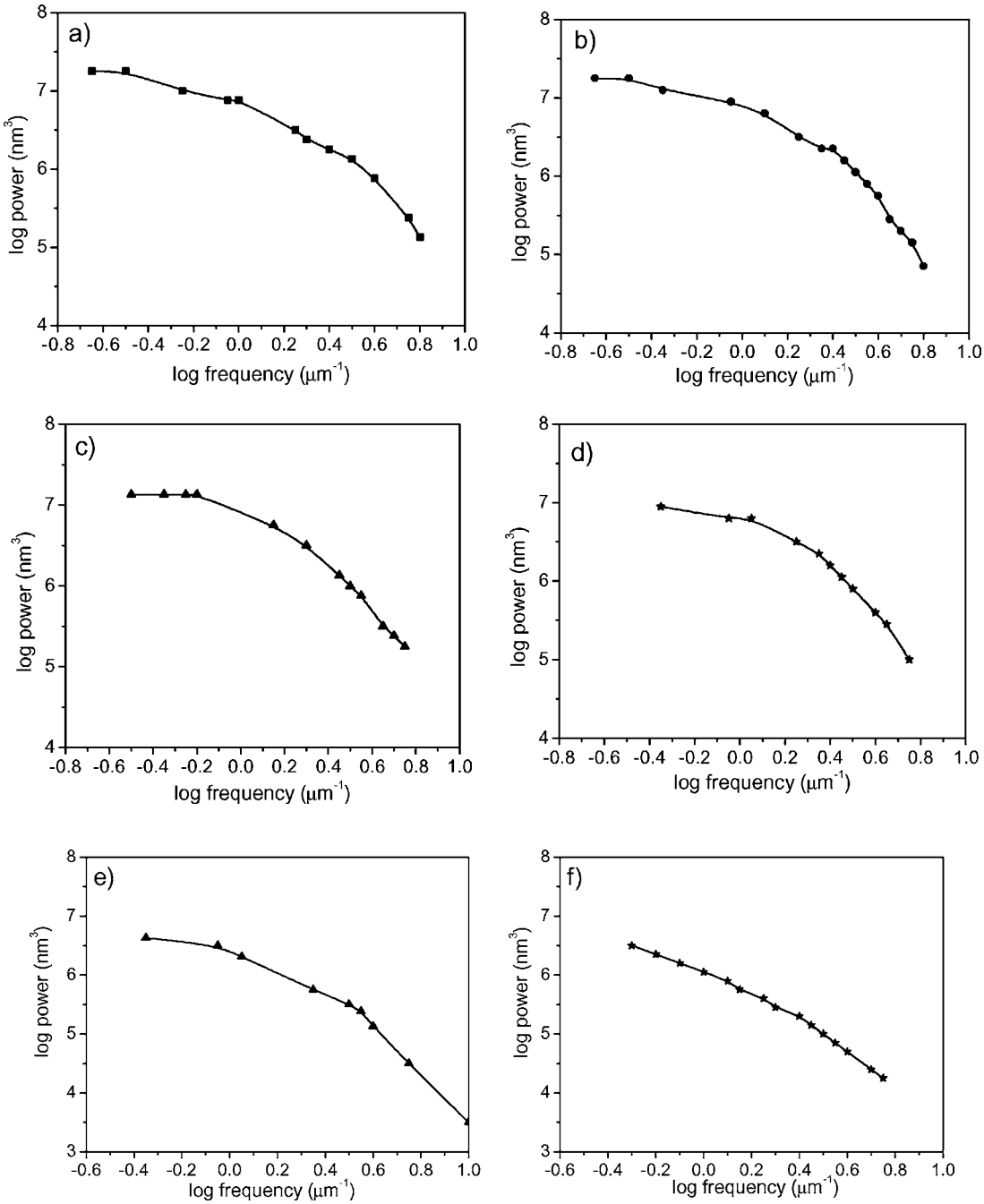

Figure 6 PSDs of the blends: (a) $B_7S_{0.75}$, (b) $B_7S_{0.75}PB$, (c) $B_7S_{0.75}PB_8$, (d) $B_6S_{0.75}$, (e) B_6, and (f) B_7.

regions were determined by linear fitting using *Origin 6.0* software. The total fractal dimensions (D_s) of the surfaces were calculated by using the following equation:

$$D_s = D + 1 \tag{6}$$

The value of D_s for a fractal surface ranges from 2 to 3. Fig. 6a–d show the 1D PSD corresponding to the images in Fig. 3a–d. The fractal values of the dynamically vulcanized blends ($B_7S_{0.75}$, $B_7S_{0.75}PB$, $B_7S_{0.75}PB_8$, and $B_6S_{0.75}$) are 2.56, 2.46, 2.45, and 2.47 respectively (Table III). The higher the fractal value, the higher will be the regularity of the shape. The shape of the dispersed particles is more regular in dynamically vulcanized blends than unvulcanized ones as is evident from the fractal (D_s) values. The fractal values of the 70/30 NBR/SAN blends are in the following order: $B_7S_{0.75}$ > $B_7S_{0.75}PB$ > $B_7S_{0.75}PB_8$. Due to this reason, the mechanical properties of the dynamically vulcanized 70/30 NBR/SAN blend prepared by the masterbatch method (Scheme 1) may be superior to those prepared by the preblending method (Schemes 2 and 3).

Fig. 6e and f show the 1D PSD corresponding to the images in Fig. 4a and b and the fractal values are shown in Table III. The fractal value of B_6 is 2.19. This shows that the surface features (i.e., dispersed phase) have nearly planar geometry. The blend B_7 have fractal dimension 2.31. The surface features of this blend can be thought of to be more regular.

The fractal values of the dynamically vulcanized 70/30 and 60/40 NBR/SAN blends are higher than those of their unvulcanized counterparts. This implies that dynamic vulcanization produces uniform and regular

shaped particles of NBR (dispersed phase) and as a result, the mechanical properties are improved.

4. Conclusions

1. The morphology of the NBR/SAN blends changes with the blend ratio. For the 60/40 NBR/SAN blend, dispersed phase morphology is observed in which NBR particles are dispersed in a continuous matrix of SAN, whereas for the 70/30 NBR/SAN blend, a co-continuous morphology is observed [from Fig. 4a and b].

2. The dynamically vulcanized counterparts of the 60/40 and 70/30 NBR/SAN blends have dynamically cured NBR particles as the dispersed phase in a continuous matrix of SAN [from TEM {Fig. 2a–d and AFM (Fig. 3a–d}].

3. The surfaces of these blends are not smooth and contain a large number of bumps and holes as are evident from their R_{ms} and R_a values.

4. Dynamically vulcanized 70/30 NBR/SAN blends prepared by the masterbatch method have higher fractal value than those prepared by the preblending method. Hence, the mechanical properties of the former are superior to those of the latter.

Acknowledgements

The authors wish to thank the Department of Science and Technology (DST), New Delhi, India for sponsoring the project. Thanks are also due to Australia-India Council, Canberra, Australia for the financial assistance in carrying out the AFM and TEM studies.

References

1. J. K. KOCSIS, in "Polymer Blends and Alloys," edited by G. O. Shonaike and G. P. Simon (Marcell Dekker Inc., New York, 1999) p. 125.
2. A. Y. CORAN, in "Handbook of Elastomers," edited by A. K. Bhowmick and H. L. Stephens (Marcel Dekker, New York, 2001) p. 249.
3. S. A. SABET, R. C. PUYDAK and C. P. RADER, *Rubber Chem. Technol.* **69** (1996) 476.
4. R. C. DUNN, G. R. HOTOM, L. METS and X. S. XIE, *J. Phys. Chem.* **98** (1994) 3094.
5. R. MCEVOY, S. KRAUSE and P. WU, *Polymer* **39** (1998) 5223.
6. H. HOSEGAVA and T. HASHIMOTO, *ibid.* **33** (1992) 475.
7. N. WINOGRAD, *Anal. Chem.* **65** (1993) 622 A.
8. R. S. MCLEAN and B. B. SAUER, *Macromolecules* **30** (1997) 8314.
9. D. RAGHAVAN, X. GU, T. NGUYEN, M. VAN LANDINGHAM and A. KARIM, *ibid.* **33** (2000) 2573.
10. D. RAGHAVAN, X. GU, M. VAN LANDINGHAM and T. NGUYEN, *Macromol. Symp.* **166** (2001) 297.
11. M. GANTER, R. BRANDSCH, Y. THOMMAN, T. MALNER and G. BAR, *Kautsch. Gum. Kunst.* **52** (1999) 717.
12. S. MASS, R. LAY and W. GRONSKI, *ibid.* **49** (1996) 166.
13. M. MOTOMATSU, W. MIZUTAMI and H. TOKUMOTO, *Polymer* **38** (1997) 1779.
14. M. C. DAVIES, K. M. SHAKESHEFF, A. G. SHARD, A. DOMB, C. J. ROBERTS, S. J. B. TENDLER and P. M. WILLIAMS, *Macromolecules* **29** (1996) 2205.
15. C. J. BUCHKO, K. M. KOZLOFF and D. C. MARTIN, *Biomaterials* **22** (2001) 1289.
16. S. GHOSH, D. KHASTGIR, A. K. BHOWMICK, S. BANDYOPADHYAY, G. J. P. GAO and L. KOK, *J. Mater. Sci. Lett.* **19** (2000) 2161.
17. R. S. RAJEEV, S. K. DE, A. K. BHOWMICK, G. J. P. GAO and S. BANDYOPADHYAY, *J. Mater. Sci.* **36** (2001) 2621.
18. S. CHATTOPADHYAY, T. K. CHAKI, A. K. BHOWMICK, G. J. P. GAO and S. BANDYOPADHYAY, *J. Appl. Polym. Sci.* **81** (2001) 1936.
19. S. ANANDHAN, P. P. DE, S. K. DE and A. K. BHOWMICK, *ibid.* **88** (2003) 1976.
20. Q. ZHONG, D. INNIS, K. KJOLLER and V. B. ELINGS, *Surf. Sci.* **290** (1993) L688.
21. M. BINGGELI, R. CHRISTOPH, H. E. HINTERMAN, J. COLCHER and O. MARTI, *Nanotechnology* **4** (1993) 59.
22. M. R. KAMAL, Z. TANG and T. HUANG, *Int. Polym. Process.* **16** (2001) 376.
23. AFM Manual, Digital Instruments, Santa Barbara, California, USA.
24. G. BAR, Y. THOMANN, R. BRANDSCH, H. J. CANTOW and W. H. WHANGHO, *Langmuir* **13** (1997) 3807.
25. S. N. MAGONOV, V. ELINGS and V. S. PAPKOV, *Polymer* **38** (1997) 297.
26. M. R. VAN LANDINGHAM, R. F. EDULJEE and J. W. GILLESPIE, *J. Appl. Polym. Sci.* **71** (1999) 699.
27. S. N. MAGONOV, V. ELLINGS and M. H. WHANGBO, *Surf. Sci.* **375** (1997) L385.

Received 30 January
and accepted 13 March 2003